Chapter 10

Systematic Effects

In this chapter, we study and quantify the various mechanisms that can contribute to systematic effects and shifts in our measurements. We classify the possible influences in accurate frequency measurements into three categories. The first category concerns imperfections in the magnetic and electric field. A second derives from imprecision in our knowledge of where the confined particles reside. A third is the degree our detection affects the unperturbed oscillations.

10.1 Deviations From a Stable, Uniform Magnetic Field

10.1.1 Homogeneity

NMR without Trap Apparatus

A pulsed NMR system is used to shim the superconducting solenoid so that a NMR linewidth is 1×10^{-8} over a 1 cm diameter spherical volume of acetone. The field is perturbed by the trap apparatus, and in particular by the trap electrodes.

With the trap in place, the proton cyclotron frequency is measured and can be compared to the proton NMR measurement if it is made in the same magnetic field by

$$\frac{\nu_c}{\nu_{NMR}} \approx \frac{1}{\gamma_p'}\left(\frac{e}{m_p c}\right) = 0.3583112 \tag{10.1}$$

where γ_p' is the gyromagnetic ratio for protons in water. The proton cyclotron measurements usually agree with the NMR measurements to within 1 part in 10^5,

depending on the actual trap apparatus and the time between the measurements. In addition to possible chemical and temperature dependent shifts in the NMR measurement, shifts at the 10^{-5} level also result from paramagnetism of the nearby trap components. (For example, using the calculated coeficient $\beta_0 \approx$-0.5 G from the MACOR spacers in the trap, paramagnetism is responsible for a shift of $\approx$ -8×10^{-6}).

Axial Displacement of the Confined Particles

The trap apparatus resides in vacuum and is cooled to 4.2 K. The volume of the confined particles is so small that to measure the field homogeneity we displace the particles up and down along the z axis and measure their cyclotron resonance to obtain information about possible magnetic field gradients.

The center of the axial oscillation is shifted by application of a small anti-symmetric dc potential $\pm V_A$ to the trap endcaps [31]. The resulting equilibrium position of the confined particle(s) is shifted from z=0 to the new position [43]

$$z_{equil.} = -\frac{d^2}{2z_0}\frac{c_1}{C_2}\frac{V_A}{V_0} = -0.2742\,\frac{V_A}{2V_0}\;cm. \tag{10.2}$$

The resonant axial frequency will also shift an amount proportional to the product c_1c_3 (where c_1 and c_3 are defined in chapter 3) given by

$$\frac{\Delta\omega_z}{\omega_z} = -\frac{3}{4}\left(\frac{d}{z_0}\right)^4\frac{c_1c_3}{C_2C_2}\left(\frac{V_A}{V_0}\right)^2 = -0.1081\left(\frac{V_A}{V_0}\right)^2. \tag{10.3}$$

Figure 10.1 shows the measured free space cyclotron frequency when antiprotons are displaced up and down by 0.5 mm in the trap. The measurement is taken by simultaneously measuring the modified cyclotron and axial frequency to determine $\nu_c(z,\rho)$ as described in Chapter 9. For comparison, we superimpose in Fig. 10.1 a linear gradient of 16 mG/cm (2.7×10^{-8}/mm) and the maximum magnetic bottle gradient based on the calculation in Chapter 3 of 1 G/cm^2 (1.7×10^{-7}/mm). The measured points demonstrate that even if the diameter of the cloud were as large as 1 mm, the gradients are not a limitation on the experiment at the level reported here. Gradient studies can also be performed by applying linear

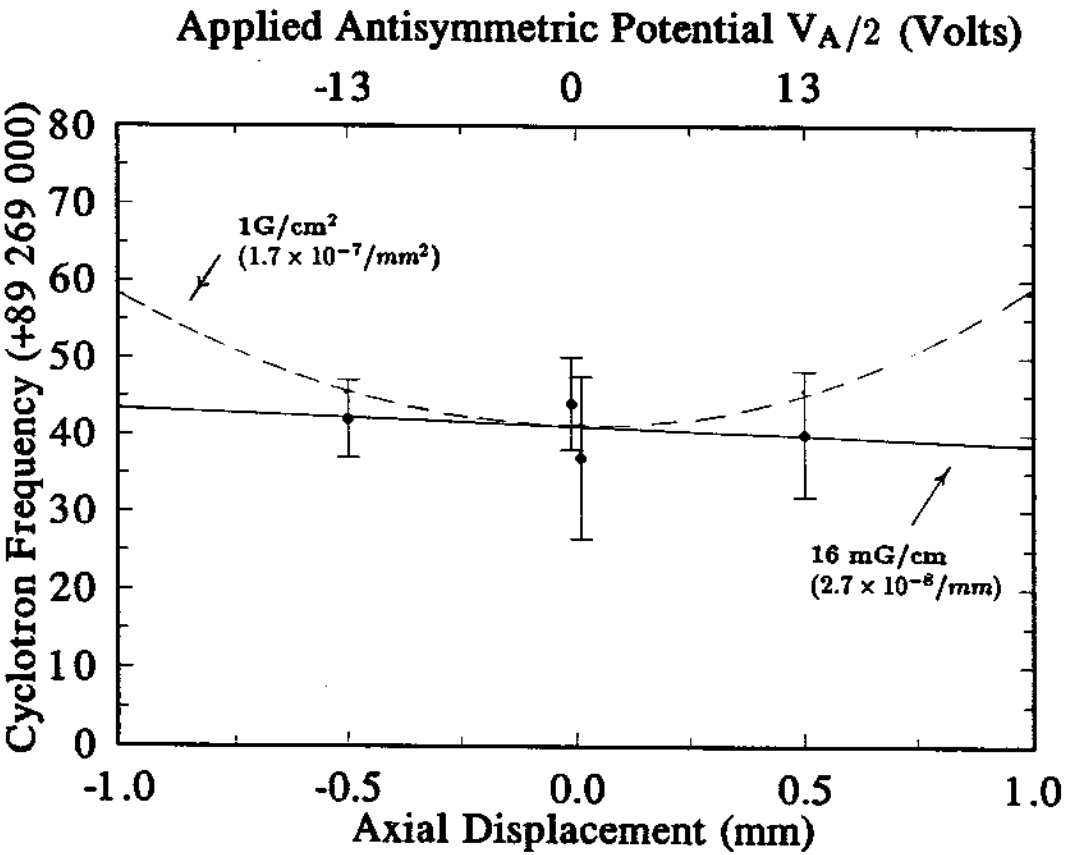

Figure 10.1: Antiproton cyclotron frequency as a function of axial location in the trap.

and quadratic gradients with the room temperature shims of the Nalorac magnet, though the maximum applied gradients of ± 1.5 G/cm and ± 0.2 G/cm^2 are too small to significantly affect our typical signals.

10.1.2 Field Drift Over Time

Average Long Term Decay

The magnetic field resulting from the persistent superconducting solenoid decreases over time. After initial energization, the solenoid is under severe stress so that over time the wires physically move small amounts until a mechanical equilibrium is reached. We attempt to reduce this time by operating the solenoid for a few minutes at a higher field than desired during energization. This has the effect of temporarily putting additional stress into the coil to speed its movement to a mechanical equilibrium. We then lower the field to the final value.

For our magnet (NCC 6.0/100/123), the decay rate $(\Delta B/\Delta t)/B$ converges to between 3 and 8 $\times 10^{-10}$ per hour after about 1 month. The field drift is shown in Fig. 10.2 using antiproton, proton, and electron cyclotron measurements over a period of three months starting with magnet energization and shimming. If mass comparisons are done over a time interval longer than the time drift of comparable precision, the drift of the magnet must be taken into account.

Internal Short Term Variations

Small variations in the drift rate occur between 3 and 8 $\times$ 10^{-10} /hour which are not directly explained by changes in the ambient field. Even though the cyclotron measurements are taken with nearly identical ambient field conditions, the measurements often reveal a short term oscillation on a time scale of 24 to 48 hours. Such fluctuations may be due to variations of the magnetic field produced by the solenoid.

Part of an explanation to the 'internal' magnetic variations may be related to an apparent correlation of the drift rate to a change of the mechanical stress on the magnet. For example, changing the on/off state of the large nearby bending

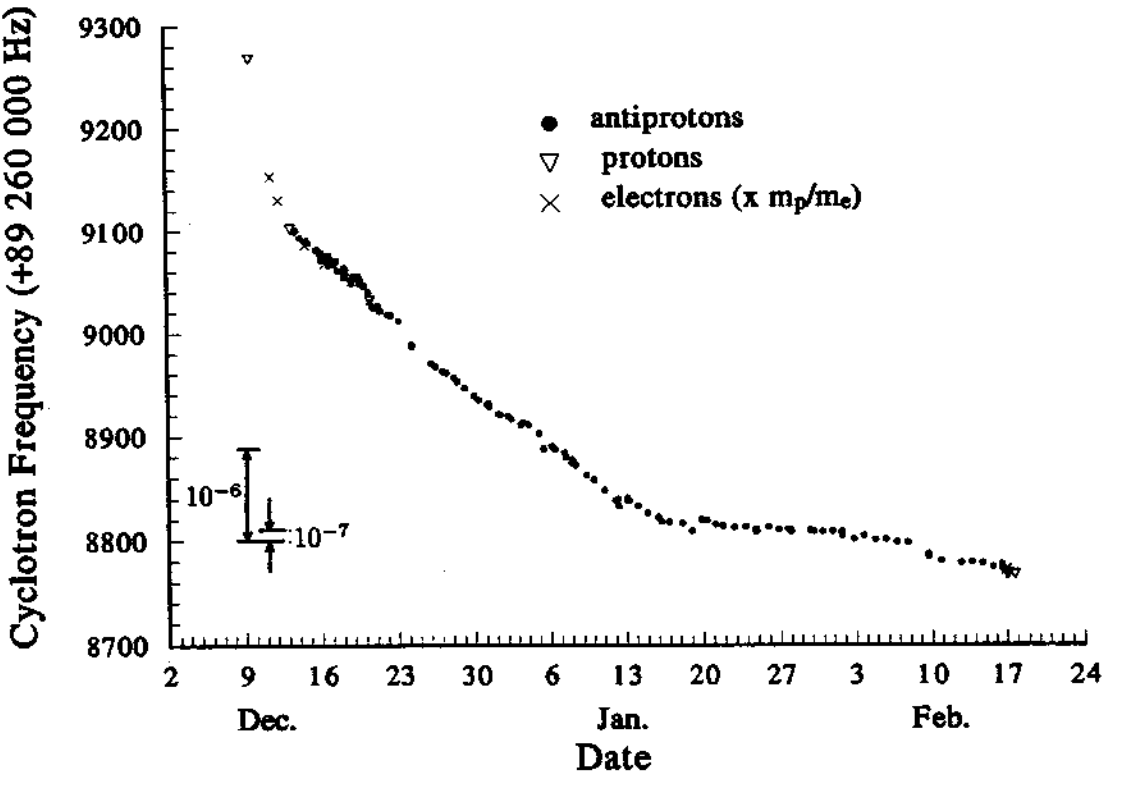

Figure 10.2: Decay of the magnetic field over several months since magnet energization on December 8^{th}.

magnet changes the stress on the solenoid so that it apparently creeps to a new mechanical equilibrium. Such a rate change can be seen in Figs. 11.1(a) and 11.2(a) which was correlated with our systematic studies of the S5 bending magnet on December 20.

We can subtract the long term drift from the measured values, but this is not totally satisfactory for short term variations. The error due to the residual local drift can be included in the uncertainty associated with the scatter of the points (chapter 11). For the highest precision measurements, the local drift must be mapped thoroughly and the time interval between comparisons should be kept to a minimum.

10.1.3 Fluctuations in the Ambient Field

Since a mass comparison between two species can take more than an hour, it is important to control short term field fluctuations that result from changes in the ambient field. In Chapter 3, we discussed the addition of a single superconducting self-shielding coil to our magnet [42] . With the scheme incorporated in our magnet, the most effective shielding is for a fluctuation in the ambient field that is uniform in the $\hat{z}$ direction. For a uniform perturbation the shielding factor increased from S=–4.27(7) (the magnet solenoid alone) to S=–156(6) with the persistent self shielding coil [46]. The shielding is less effective for magnetic gradients, and as a result, each magnetic source in the experimental hall is shielded differently.

In Table 10.1, we summarize the maximum field fluctuations observed outside and inside the shielded magnet system located in an experimental hall at CERN. The outside field fluctuations are measured using a Schonstedt DM2220 Magnetometer rigidly mounted approximately 1.5 meters from the high field solenoid. In Fig. 10.3 the major field fluctuations are shown as a function of time and several sources are identified.

The fluctuations at the trap location in the magnet bore ΔB_{int} are measured at room temperature with a magnetometer (Fig. 10.4), or in most cases with cyclotron resonance measurements of electrons and antiprotons (Fig. 10.5). We

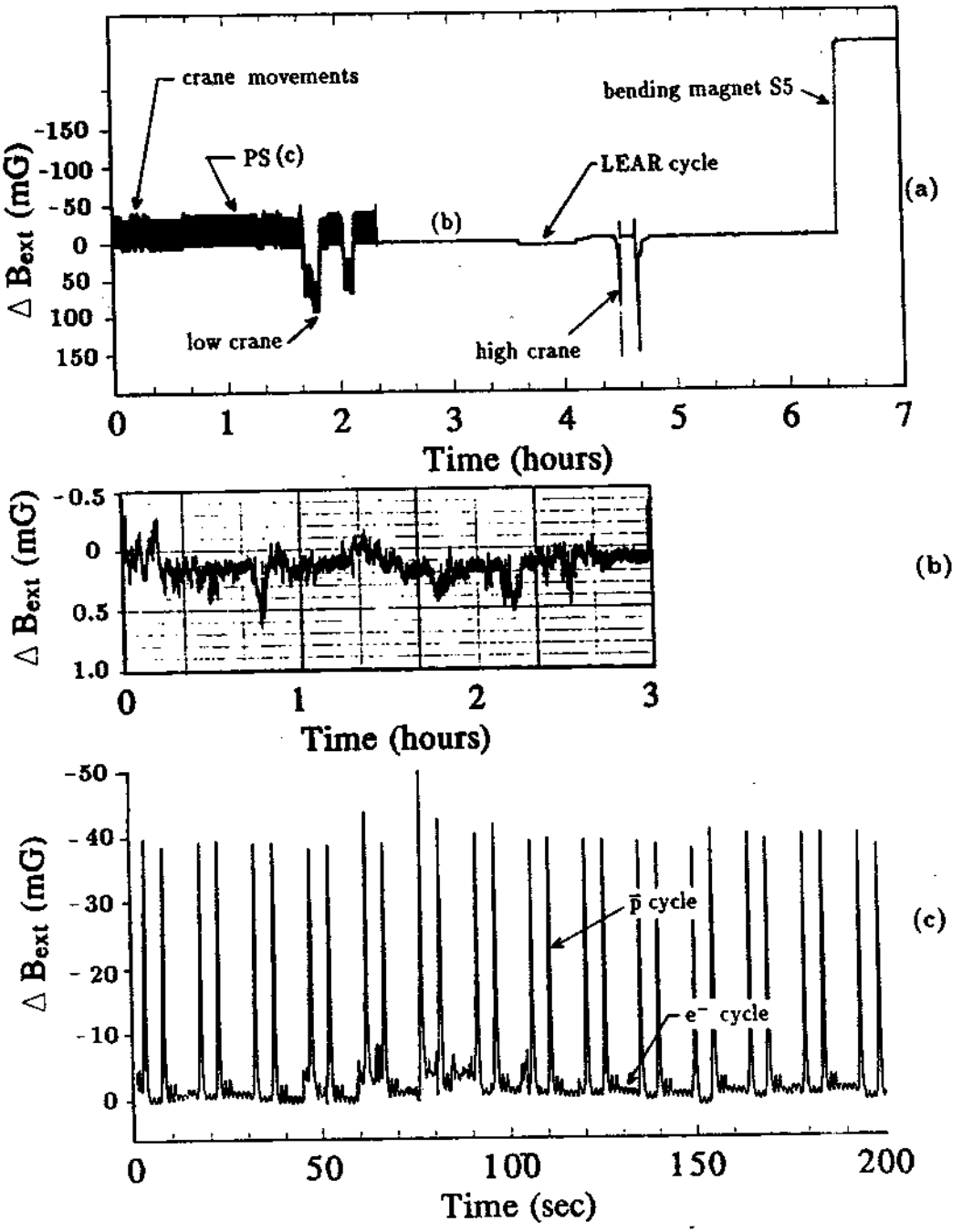

Figure 10.3: (a) Several of the major field fluctuations identified in the experimental hall 1.5 m from the trap. (b)Amplified measurment of fluctuations during a quiet period with the accelerator magnets off. (c) Expanded view of the PS cycle.

Table 10.1: Summary of the external magnetic perturbations. All values are with respect to magnet 'off' values. The magnet 'on' state refers to a polarity for antiprotons.

Source	ΔB_{ext} [mG]	ΔB_{int} [mG]	$S = \frac{B_{ext}}{B_{int}}$	$\frac{\Delta M}{M}$
S5 Mag.(on)	+230	8.3	≥ 27	1.4×10^{-7}
S4 Mag.(on)	+173	2.8	≥ 60	4.8×10^{-8}
High Crane(above)	+146	≤ 3	≥ 50	5×10^{-8}
Low Crane(beside)	+88	≤ 1.2	≥ 75	2×10^{-8}
PS (P cycle)	-37	0.33*	110	6×10^{-9}
PS (e^- cycle)	-3	–	110	5×10^{-9}
LEAR (cooling)	+19	0.4*	50	7×10^{-9}
ΔB_{earth}(max.)	≤ 5	–	≈ 156	5×10^{-10}

* Measured with magnetometer with magnetic field off but solenoid and shield superconducting.

also quantify the approximate shielding effectiveness for each source and tabulate the fractional systematic shift that each source contributes to a cyclotron (mass) measurement. When the internal field is measured with a magnetometer, the finite size of the probe may limit the observed shielding factor. Also for the cases of bending magnets S4 and S5, the solenoid is closer to the source than the magnetometer to measure the external field. Therefore the shielding we report is the minimum factor observed and it may actually be larger in some cases.

A few comments about the largest field shifts follow.

- S-5 Bending Magnets for 5.9 MeV Antiprotons

  Two 45 degree bending magnets, with a quadrupole between, are a part of our beam line. The upper segment ends less than 1 meter from the center of our high precision trapping field. Even though the magnet being on or off is the largest magnetic perturbation in the hall, the shielding limits this shift to only $\Delta\nu_c'/\nu_c' = 1.4 \times 10^{-7}$ at the magnet center. The on/off state of these magnets is under our direct control since it is only in our beamline. Therefore we can make sure that the field remains constant during the measurement.

- S-4 Bending Magnets

$$S_{PS} = \frac{\Delta B_{ext}}{\Delta B_{int}} \approx -110 \qquad S_{LEAR} = \frac{\Delta B_{ext}}{\Delta B_{int}} \approx -50$$

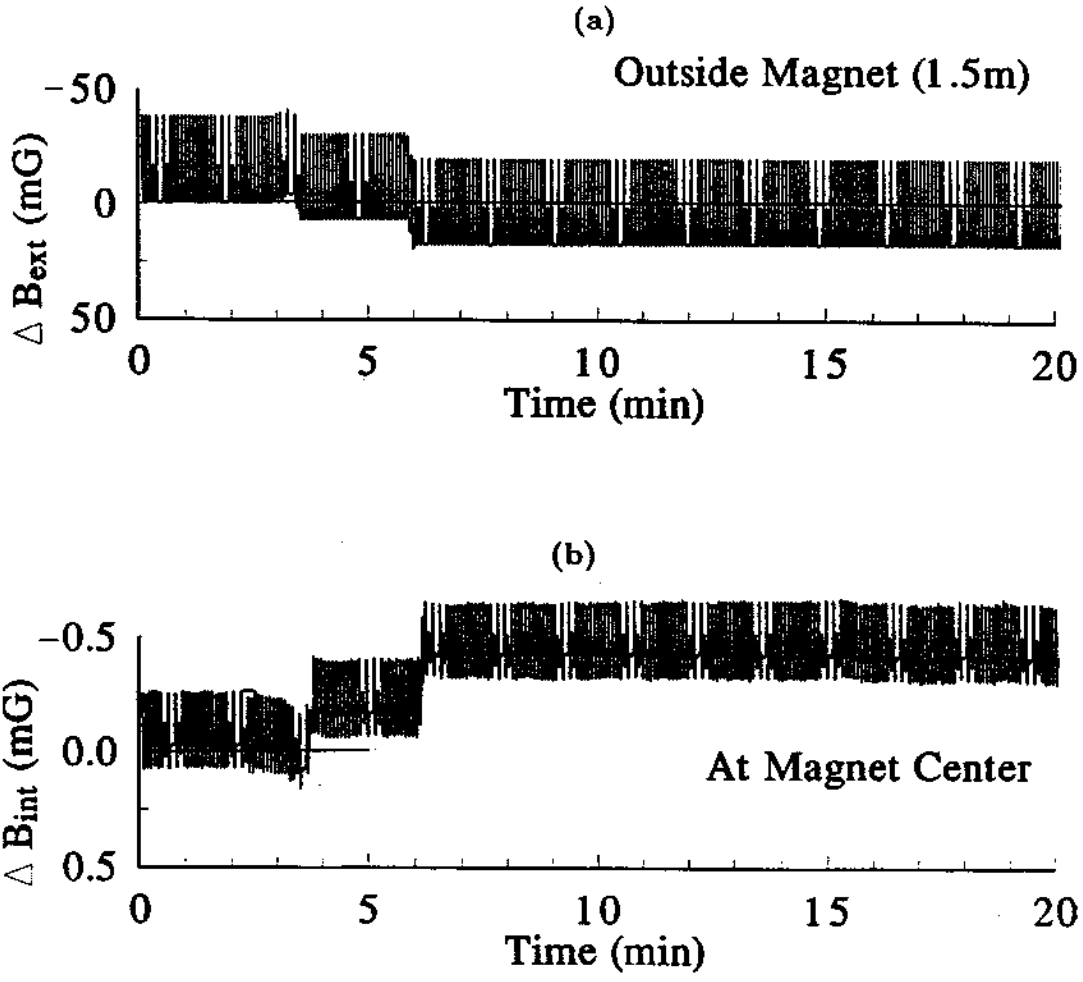

Figure 10.4: Magnetic Fluctuations from the CERN Proton Synchrotron superimposed on a LEAR deceleration cycle. (a) Measured with a magnetometer outside of the magnet and (b) measured with an identical magnetometer inside the self shielding solenoid.

$$S_{S4} = \frac{\Delta B_{ext}}{\Delta B_{int}} \geq -60$$

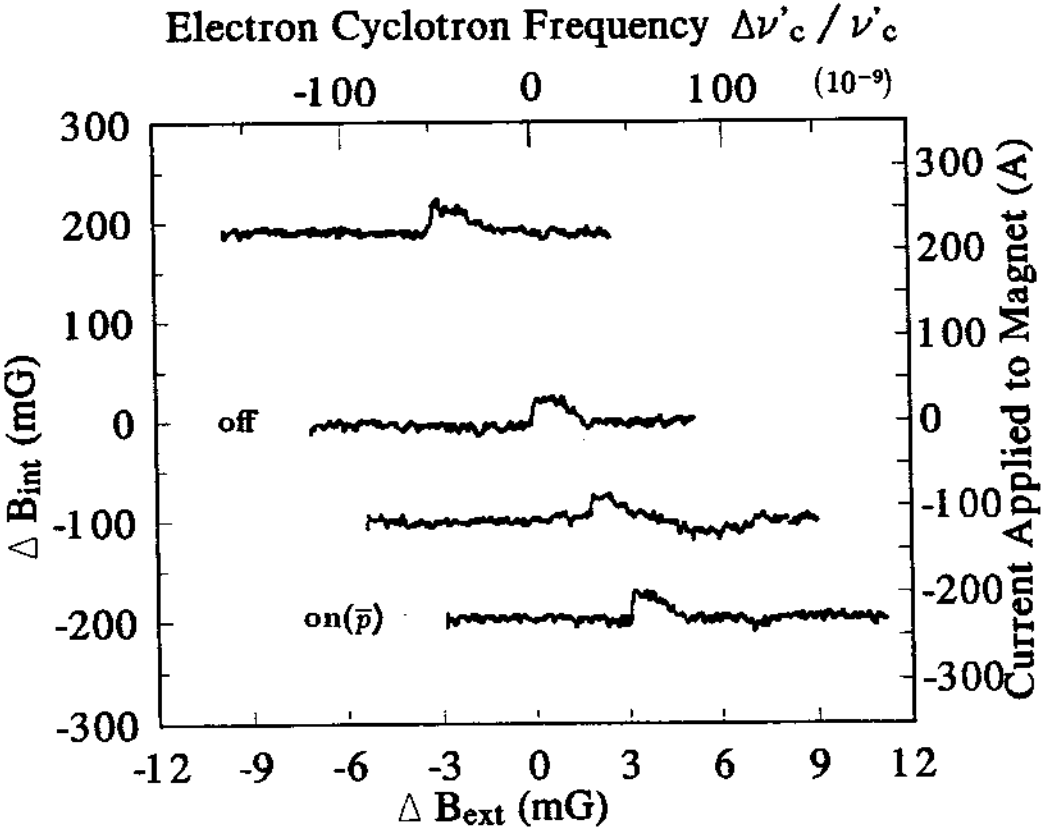

Figure 10.5: The magnetic field shift due to bending magnet S4-BHN01 at the trap center as measured by a shift in the electron cyclotron resonance.

A beamline adjacent to our experiment has an identical 45° bending magnet as in our beamline except that it is horizontal and is slightly further away. This beamline was installed after the data presented in chapter 10 was taken. The absolute shift from the off/on state of this magnet is $\Delta\nu_c/\nu_c = +4.8\times10^{-8}$ (Fig. 10.5). The rest of the beamlines in the experimental hall consist of much smaller bending magnets and quadrupoles and are not visible at the 10^{-9} level.

- Steel Overhead Cranes

  Two very large steel cranes can move as close as 1.5 meters from the magnet. Both cranes are normally stored far away from the experiment. A high crane can move over the top of the experimental region (see Fig. 3.10) and a lower crane can move up beside it. The largest systematic shift due to the cranes are $\Delta\nu_c'/\nu_c' \leq 3x10^{-8}$ in the shielded solenoid.

  Mass comparisons are not done when the cranes are moving, or near the experiment. Typically the cranes only operate extensively during accelerator shutdowns when no antiprotons are available. When antiprotons are available, the cranes are seldomly used, and if so are usually limited to Weekdays, 8:00 am to 5:00 pm.

- CERN Proton Synchrotron (PS)

  The magnets of this accelerator-decelerator ring are typically ramped every 2.4 seconds (see Figs. 10.4 and 10.3) when high energy protons are accelerated for the the Antiproton Accumulator (AA), the East Hall, or the Super Proton Synchrotron (SPS). The fluctuation is fast and is partially screened by eddy currents in the solenoid spool [42]. In a worse case scenario, if the fluctuation were a dc field shift, $\Delta\nu_c'/\nu_c'$ would be a shift less than $5x10^{-9}$ or about 0.5 Hz. We note that the magnitude of the frequency shift is about the same as the modulation frequency of 2.4 seconds. Since the modulation index is high, it may be possible that the observed cyclotron resonance line is broadened by the existence of FM sidebands.

  The PS cycle to fill the Large Electron Positron collider (LEP) uses much

smaller magnetic fields as seen in Fig. 10.3(c). For measurements at the 10^{-9} level, possible perturbations from the PS can be avoided by field monitoring and measurement timing.

- CERN Low Energy Antiproton Ring (LEAR)
  The LEAR decelerator ring is about 10 meters from our magnet and is observable during the antiproton load and deceleration cycle in LEAR (see Figs. 10.4 and 10.3(a)). This cycle occurs for about 15 minutes once every 3 hours. Since the maximum field perturbation in the shielded magnet is about $\Delta\nu_c' / \nu_c' = 6\text{x}10^{-9}$, this cycle will have to be avoided during measurements at the highest precisions.

By monitoring the magnet time drift and the major external perturbations (mainly the on/off state of the antiproton beamline bending magnets) the magnetic field systematics are not relevant for comparisons at the 4×10^{-8} level. The gradients are sufficiently small that the accuracy of our measurements are not compromised, even if the cloud has the very large spatial extent of 1 mm^3. For a spherical shaped cloud the effect of the calculated bottle would be at most 2×10^{-8}. The cloud dimensions for reasonable energies are typically much smaller. A broadening due to possible linear gradients is less than 10^{-8}/mm. Small magnetic gradients result from our use of a large trap and also because the magnet bore can be operated at room temperature making it possible to shim away external gradients to high precision over a large volume (0.5 cm^3) using an NMR probe. This later feature is especially meaningful in our application since very large magnetic perturbations close to our solenoid must be compensated (for example, reinforced concrete shielding and bending magnets).

By avoiding the major external field fluctuations, summarized in Table 10.1 , they are not relevant at our present level of accuracy. As the mass comparison progresses to higher precision, the external fluctuations become more critical, but should be manageable with proper measurement timing or active external correction. The short term time variation of the field is best monitored with cyclotron measurements made as close together in time as possible. For the purpose of our

comparisons, these variations are small and are incorporated into the analysis in Chapter 11 as an uncertainty associated with scatter.

10.2 Deviations From the Pure Quadrupole Electric Field

Magnetic perturbations described in the previous section affect ν_c' to first order but have little effect on ν_z . Electric field perturbations affect all three eigenfrequencies. In an ideal trap, a change in any of the eigenfrequencies will be accompanied by corresponding changes in the other two so that ν_c is invariant to such changes. In this section, we put limits on perturbations from the ideal quadrupole potential that can have an effect on the accuracy of our measurements of the free space cyclotron frequency.

10.2.1 Trap Geometry and Alignment

Orthogonalized Cylindrical Traps

The open endcap trap, described in chapter 3, was designed and constructed so as to produce a sufficiently high quality quadrupole potential at the trap center. High precision measurements are possible only because particles in thermal equilibrium with 4 K typically have small orbits. Away from the center of the trap, the approximation that the cylindrical trap forms a pure quadrupole potential begins to break down. As a result, particle energies should be as low as possible during resonance detection.

Trap Distortions and Misalignments

The invariance theorem given by (2.19) serves as a prescription to determine the free space cyclotron frequency in terms of the real measured eigenfrequencies $\overline{\nu}_c'$, $\overline{\nu}_z$, $\overline{\nu}_m$ of a single particle in a non-perfect trap.

This expression can be expanded in terms of a distortion parameter ϵ and

misalignment angle θ [13], giving

$$\frac{\omega_c}{\overline{\omega}'_c} = 1 + \frac{1}{2}\left(\frac{\overline{\omega}_z}{\overline{\omega}'_c}\right)^2 + \frac{9}{16}\left(\frac{\overline{\omega}_z}{\overline{\omega}'_c}\right)^4 (\theta^2 - \frac{2}{9}\epsilon^2) + ... \qquad (10.4)$$

which we identify as $\nu_c = \overline{\nu}'_c + \overline{\nu}_z{}^2/2\overline{\nu}'_c$ with an additional term as a function of ϵ and θ.

For our rather large 1.2 cm diameter trap $(\overline{\omega}_z/\overline{\omega}'_c)^4 = 2\times10^{-7}$. The trap was machined with tolerances of 5 μm (0.0002"). The maximum angle that the trap could be tilted with respect to the magnetic field is 0.3°. (assuming the apparatus is shorted to the wall of the magnet bore). Since the magnet bore is not directly connected to the solenoid it is possible that the solenoid is not perfectly aligned with the bore. If we assume the conservative values of ϵ=1% or $\theta = 1°$, the last term in Eq. 10.4 is still only $\Delta\nu_c = 3.6\times10^{-11}$. Therefore, the imperfections of the trap electrodes and internal and external misalignments do not contribute a significant systematic and a measurement of ν'_c and ν_z is totally sufficient to infer the free space cyclotron frequency well beyond the 10^{-9} level.

The invariance theorem was derived for the case of a single particle in a Penning trap with imperfections to the trapping potentials resulting from the actual electrodes and their alignment. For more particles, deviations from ideal quadrupole field resulting from the presence of other charges in the trap must be examined.

10.2.2 Field Effects From Electrode Potentials

For a distortion free, perfectly aligned trap containing no particles, the resulting electric field depends upon characteristics of the potential applied to the trap electrodes. This includes the quality of the voltage source, the electrode surface quality, and the absolute potentials applied to the various trap electrodes.

Stability and Accuracy of the DC Potential

Assuming the absolute worse fluctuations in the unfiltered voltage source of $\Delta V_0 = 150\mu$V then $\Delta\nu_z/\nu_z = 10^{-6}$ and $\Delta\nu_c/\nu_c = -\Delta\nu_m/\nu_c = -(\nu_z/\nu_c\nu'_c)\Delta\nu_z \approx 2\times10^{-8}$.

Symmetric Perturbations: Anharmonicity

The shape of the axial potential well is tunable using the set of compensation electrodes. For a trap that is symmetric axially and about the plane z=0, only even order terms are present in the multipole expansion in equation 3.1.

Using the notation from Chapter 3, anharmonicity in this context refers to the presence of higher even order terms in the trap potential with coeficients $C_4, C_6, C_8, ...$, where $C_k = C_k^{(0)} + (V_c/V_0)D_k$. By the nature of a trap formed with cylindrical electrodes, the trap cannot be made harmonic over all interior regions. Thus the effect of anharmonicity strongly depends on the spatial extent motion of the particles.

All mass comparison measurements were performed with the compensation potential set at 88.09% of the potential applied to the ring with the endcaps grounded. This is the theoretical setting which produces $C_4 = 0$ and $C_6 = 0$ at the trap center. Our measurements on electrons, protons, and antiprotons have indicated that $V_{comp} = 0.8809V_0$ is nearly the optimum tuning for well cooled and center particles (e.g. see the electron traces in Fig. 6.4).

We measure the effect of anharmonicity on our measurements of the antiproton cyclotron frequency by deliberately mistuning the trap. Figure 10.6 shows a series of measurements of ν_c as a function of changing the trap compensation potential ratio V_{comp}/V_0. Because the trap is not perfectly orthogonalized, mistunings of V_{comp}/V_0 result in small shifts of the axial frequency accompanied by a shift in the measured ν_c' . For a perfect trap, ν_c is invariant to these shifts since $\nu_c = \nu_c' + \nu_m$ where $\nu_m = {\nu_z}^2/2\nu_c'$. Any shift in ν_c is an indication that the anharmonicity is large enough so that these relationships are no longer valid. Even with the trap mistuned so that $C_4 = 3 \times 10^{-3}$ no correlation with a shift in ν_c is observed with the present resolution. Similarly, with the electron cyclotron measurements with a trap mistuning producing $C_4 = 5.6 \times 10^{-3}$, no correlated shift in ν_c is observed (see Fig. 6.4).

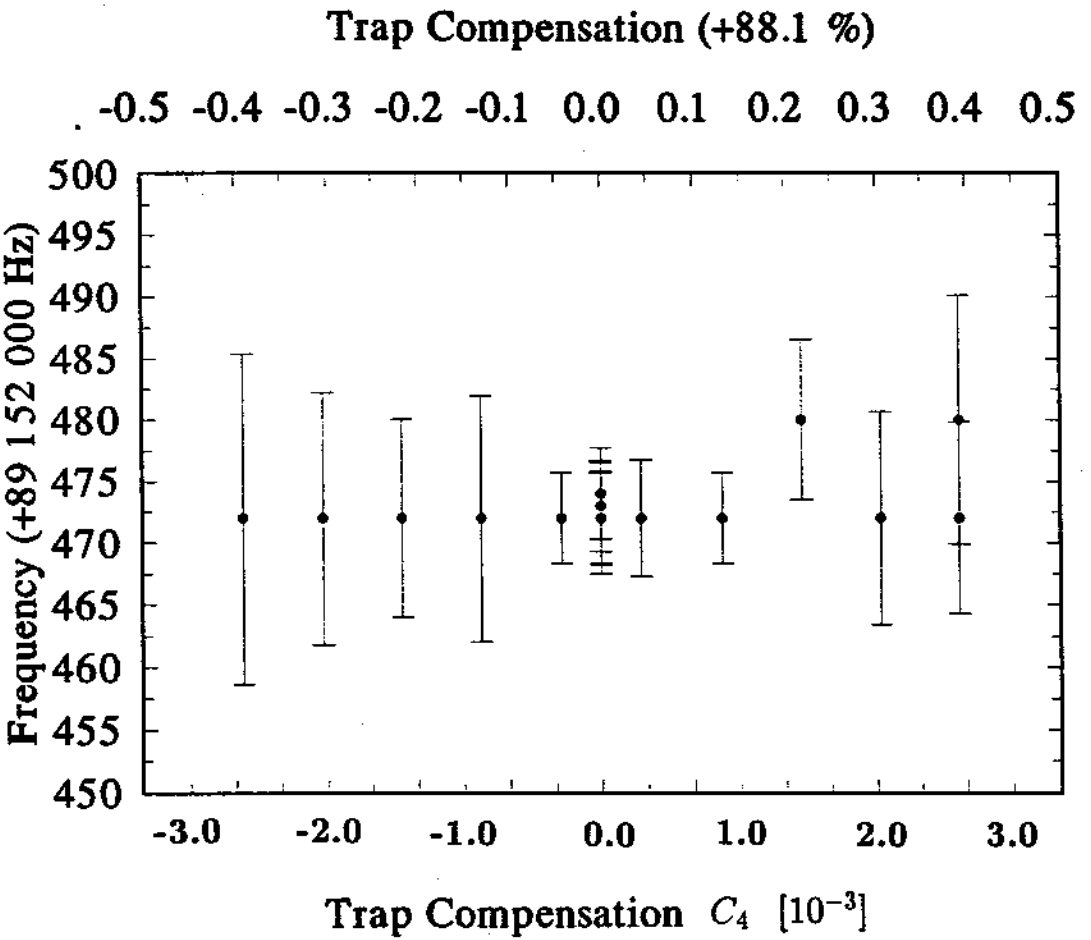

Figure 10.6: Antiproton cyclotron frequency as a function of trap compensation.

Asymmetric Perturbations: Contact Potentials and Patch Effects

Asymmetric potentials can be intentionally introduced as described in Section 11.1.2 to displace the average position of the particles in the trap. Unfortunately, small unintentional shifts can result from asymmetric potentials applied to the trap electrodes by mechanisms such as contact potentials, patch effects, or stray charges that may be present on the surface of the electrodes.

If particles are electrostatically shifted, then opposite polarity particles are displaced in the opposite direction. Such shifts could have major consequences if the electric or magnetic field significantly differs in the two regions since our comparison technique relies on the particles experiencing the same field.

In Fig. 10.7 we show evidence that the actual potential on the trap is not the same as the applied potential from the Fluke 5442A supply. We show measurements of ν_z for both antiprotons and protons with the same applied trapping potential (except opposite in sign) and the identical compensation tuning. The spectrum analyzer scales are identical in both traces. The antiproton axial frequency for the antiproton is higher than for the proton. In Fig. 10.7 we also compare measurements of ν_c' . Here we observe that the antiproton ν_c' is lower than the protons (The measurements were taken over a time where the magnetic field drift is negligible). The free space cyclotron frequency $\nu_c = \nu_c' + \nu_m$ is invariant to the voltage offset suggesting that shifts in ν_z and ν_c' result from different trapping potentials.

We determine the size of this offset potential from

$$\omega_z^2 = C_2 \frac{eV_0}{md^2} \equiv \alpha V_0, \tag{10.5}$$

so that a shift in the axial frequency as a function of only voltage is

$$\frac{\Delta\omega_z}{\omega_z} = \frac{1}{2}\frac{\Delta V_0}{V_0}. \tag{10.6}$$

Let V_{cp} denote the offset potential, then (10.5) becomes for the antiproton and proton respectively

$$(\omega_z^2)_{\bar{p}} = \alpha(|V_0 + V_{cp}|) \tag{10.7}$$

Antiprotons

14:00

$V_0 = +71.6\ V$

$V_c = 0.881\ V_0$

Protons

17:00

$V_0 = -71.6\ V$

$V_c = 0.881\ V_0$

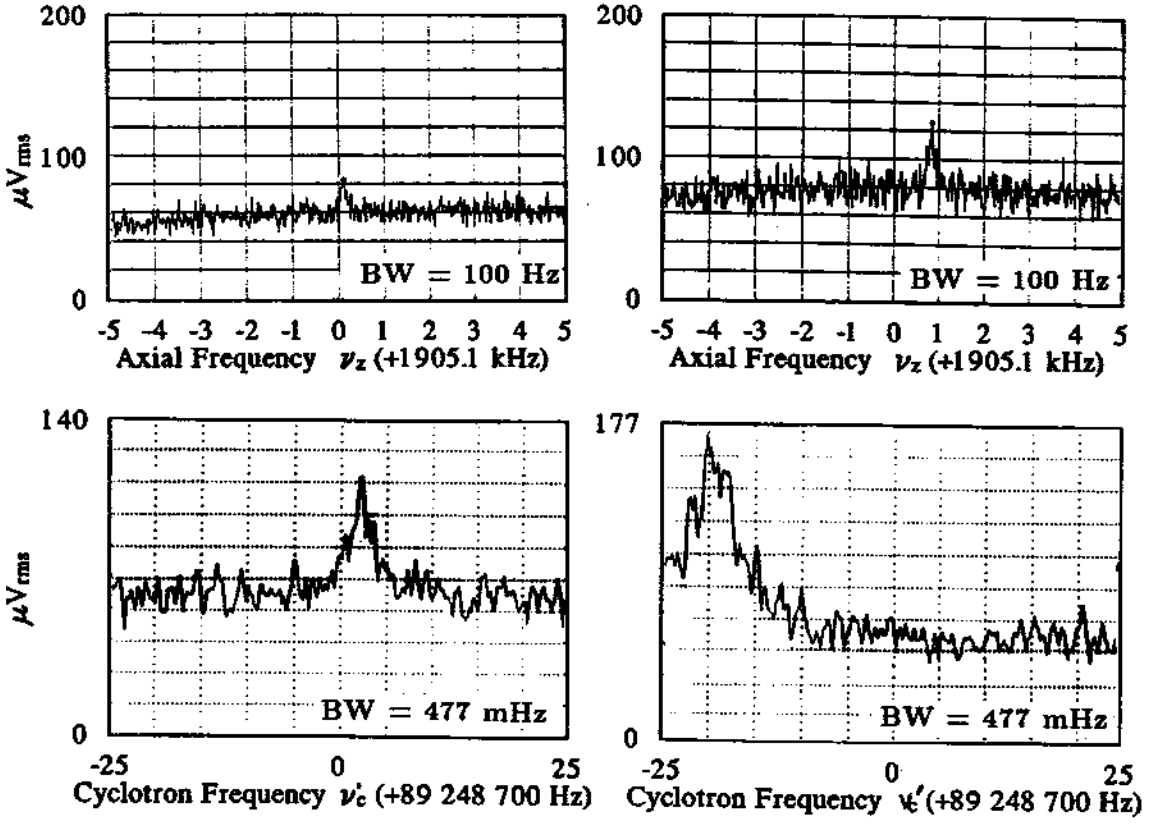

$$\Delta\nu_z = \frac{+}{2}\frac{730}{2}\ \text{Hz}$$

$$\Delta V_0 = 27 \pm 5\ \text{mV}$$

Figure 10.7: Antiproton and Proton axial and cyclotron resonances showing the effect of reversing the trapping potential.

and

$$(\omega_z^2)_p = \alpha(|V_0 - V_{cp}|). \tag{10.8}$$

Solving these two equations using the values observed in Fig. 10.7 for the axial frequencies gives an offset potential of

$$V_{cp} = 27 \pm 5mV. \tag{10.9}$$

This amount of offset could easily be a contact potential, since the dc lines from the Fluke voltage supply to the trap electrodes consist of constantan, copper, and tin-lead. There also exists a temperature gradient of approximately 300 K.

This offset, as observed through the axial frequency of the antiprotons and protons, is reproducible even if the trap apparatus has been warmed up and cooled down again. Therefore, it most likely is not due to stray surface charges which may not be so reproducible. The trap electrodes are plated with a thin layer of gold and a patch effect may be a possibility.

The axial frequency shift is most sensitive to the effect on the harmonic potential. Displacements (dependent upon c_1 or d_1) of the confined particles could result from asymmetric perturbations and the 27 mV offset gives an approximate scale of such possible perturbations. In a worst case scenario we assume that there exists a 100 mV offset between the compensation electrodes. Then using Eq. 10.2 (except now we use d_1 and d_3 since the potential is applied to the compensation electrodes) the maximum particle displacement along the z axis would be $\Delta z \approx 1.5\mu m$. Similar displacements in Δx or Δy could occur by potential offsets across segments of the split compensation or the quad ring electrodes. Our magnetic gradients are sufficiently small that displacements on this scale are insignificant.

Finally, correcting the applied voltage with this offset, we get a measure of the trap coeficient α relating ω_z^2 and V_0 as defined in Eq. 10.5 to be

$$\nu_z(p,\overline{p})_{meas.} = 0.22594\frac{MHz}{\sqrt{Volt}} \tag{10.10}$$

compared to the theoretical value for our trap dimensions [43] of $\nu_z(p,\overline{p})_{calc.} = 0.22477\frac{MHz}{\sqrt{Volt}}$. This is in agreement to 0.5% as would be expected based on the machining tolerances of the trap. This is the same level of agreement obtained

with the actual and calculated values for D_2. The calculation does not include the effect of the splits in the ring and compensation electrodes and also does not take into account the inner surfaces along the gaps between electrodes.

10.2.3 Field Effects from the Presence of Other Particles

For the highest precision mass spectroscopy even a single ion can lead to a perturbations in the measured eigenfrequencies [104]. The measurements reported in this thesis are done with more than one particle and sometimes the clouds contain other particle species. Antiprotons may be accompanied by residual electrons from the cooling process and protons accompanied with other positive ions (most often carbon, oxygen, and nitrogen). The electron measurements are most likely with single species clouds since negative ions are relatively hard to generate and are only weakly bound.

We distinguish between the perturbations caused by the number of a pure species and the perturbations due to the space charge of other ions sometimes present in the trap.

Number Dependence: Image Charge Field

The number dependence reported as a systematic in earlier measurements on the proton to electron mass ratio vary greatly in magnitude and direction [98,53]. At the time, the determined correlation to particle number may have been more related to the uncertainty in cloud volume which can also result from a number dependency. For example, a large number of particles could sample a larger trap volume and possibly sample field regions with different anharmonicity and/or magnetic bottle properties.

A model first proposed by Wineland and Dehmelt [115] is useful towards understanding the source of number dependence shifts. They model the trap electrodes as a parallel plate capacitor, with plate separation d, and interpret the number dependent perturbation as a result of the field produced at the trap center due to the image charge of the confined particles reflected about the conducting surfaces.

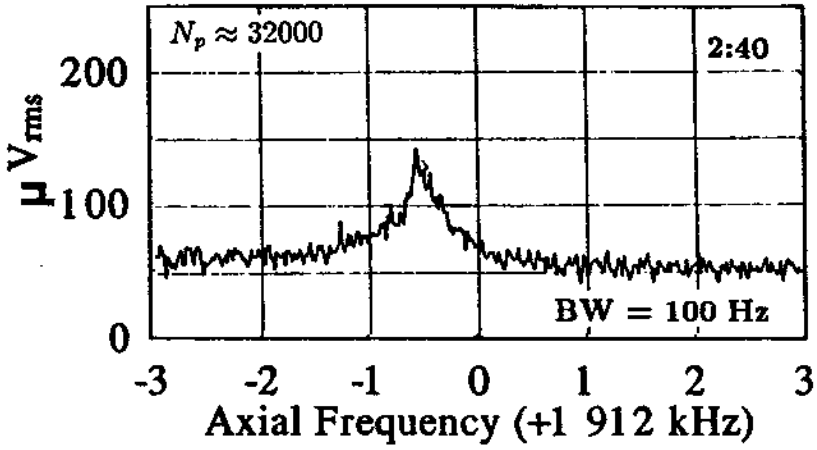

dip to -1.5 V on ring

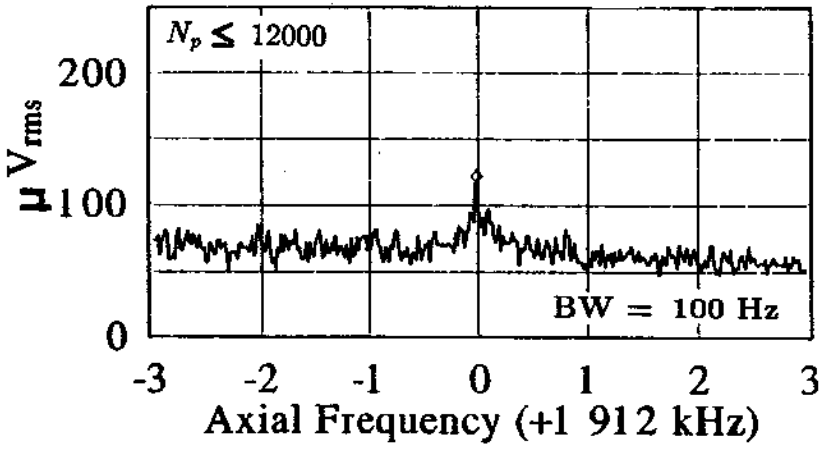

Figure 10.8: Axial shift for protons when reducing particle number in the trap. The axial signal (a) before and (b) after a drive a dip procedure to reduce proton number. The axial frequency increases for reduced particle number.

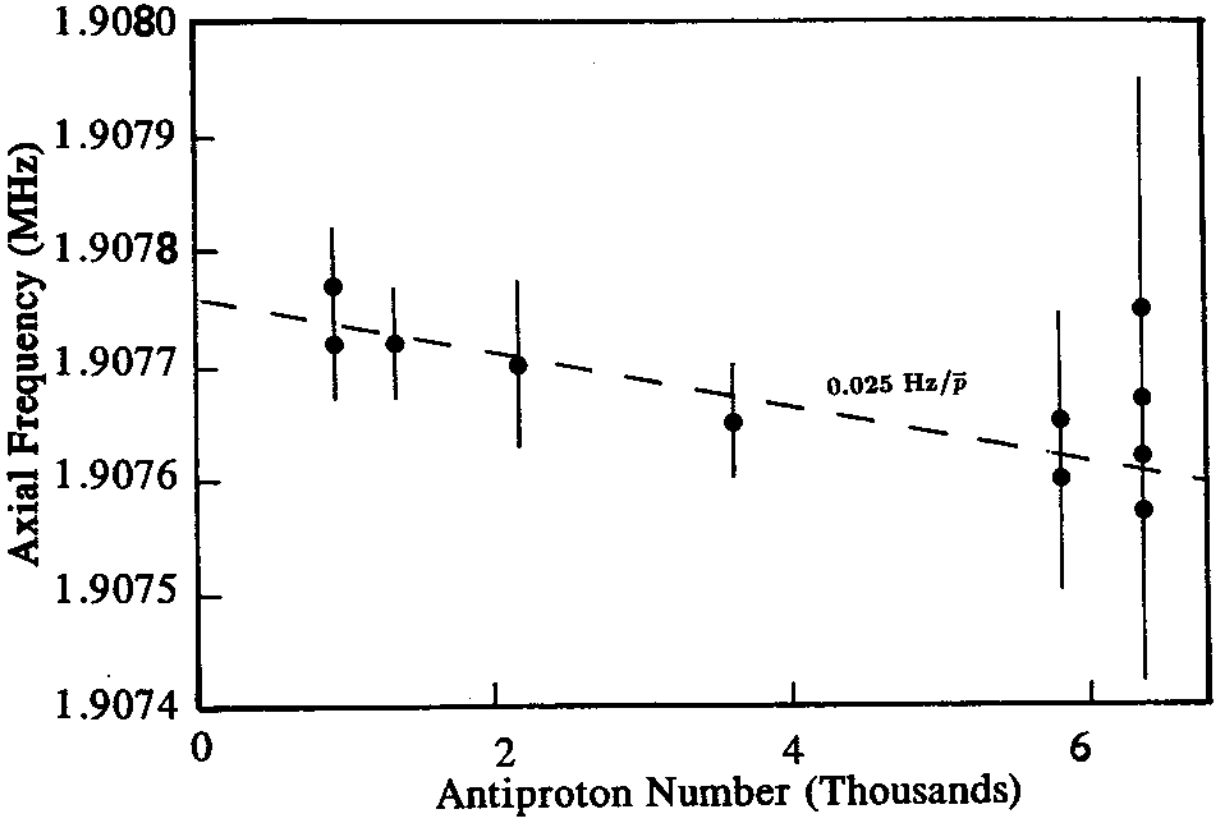

Figure 10.9: Axial shift for antiprotons as a function of the drive and dip procedure to reduce the antiproton number in the trap.

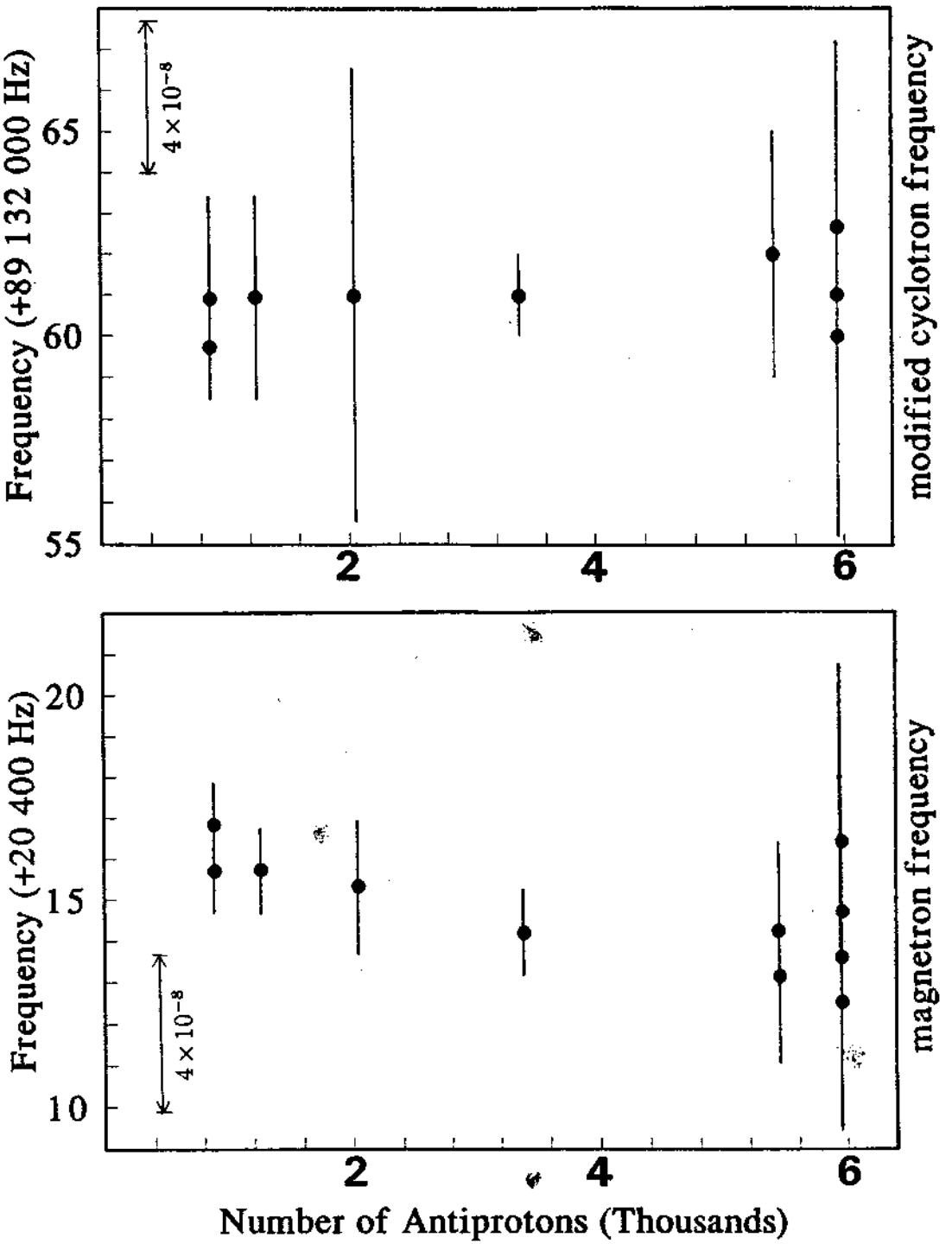

Figure 10.10: (a)The dependence of the magnetron frequency $\nu_z^2/2\nu_c'$ on particle number. (b) The dependence of the modified cyclotron frequency ν_c' on particle number.

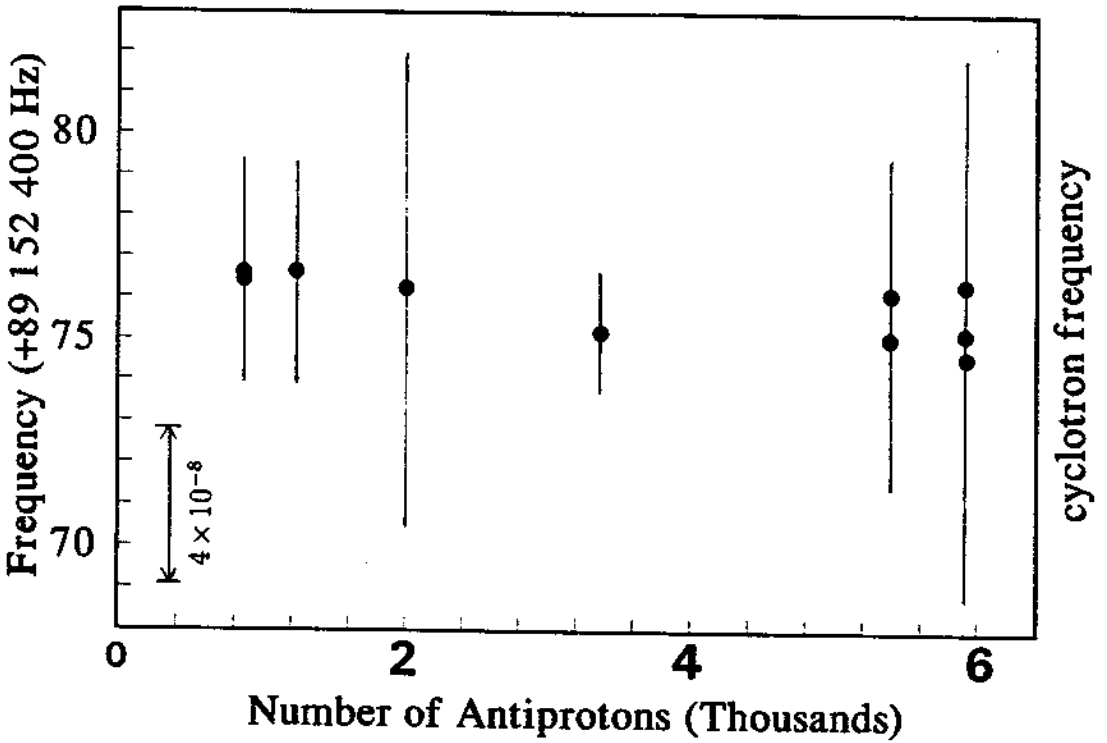

Figure 10.11: Measured antiproton cyclotron frequencies as a function of number of antiprotons in the trap.

With this model they determine the shift in the axial frequency to be

$$\frac{\Delta\omega_z}{\omega_z} = -4\frac{ne}{dV_0}, \tag{10.11}$$

where N is the number of charges e in the trap. This expression can simply be understood as the ratio of the potential produced by the image charge at the trap center ($\propto ne/d$) to the potential applied to the trap V_0.

Using Eq. 10.11 and the characteristic dimension of our trap as an approximate distance scaling, we estimate the axial frequency shift in our trap to be of order

$$\frac{\Delta\omega_z}{\omega_z} \approx -0.03Hz/\bar{p}. \tag{10.12}$$

This agrees favorably with the observed shift using antiprotons as shown in Fig. 10.9. In Figs. 10.8(a) and (b) we show the axial shift (and linewidth) change of protons as a function of number from about 3×10^4 to significantly fewer. The axial signal shifts down in frequency for increased particle number.

The image charge model has been experimentally studied by VanDyck et. al. [104]. The number dependent shifts on the magnetron and modified cyclotron frequencies within a spherical conducting cavity of radius a are quantified. Aside from a geometrical factor, the axial shifts are the same as Eq. 10.11.

The relative shift in the observed magnetron frequency scales as the total trapped mass nm_1, and is independent of charge as [104]

$$\frac{\Delta\nu_c'}{\omega_c'} = \left(\frac{3m_1c^2}{2a^3B_0^2}\right)n. \tag{10.13}$$

VanDyck et. al. measure a number dependence in the measured modified cyclotron frequency of 0.23×10^{-9}/proton. For our trap, which is effectively 3 times smaller, the relative magnetron shift should be reduced by a factor of a^3 to as

$$\frac{\Delta\omega_c'}{\omega_c'} \approx 6 \times 10^{-12}/proton. \tag{10.14}$$

Therefore, a 10^{-8} shift may result from about 1700 antiprotons (See Fig. 10.10). A nearly equal but opposite shift occurs in the modified cyclotron frequency as in the magnetron frequency, thus the free space cyclotron frequency is not particularly sensitive to number dependency. The measured free space cyclotron frequency shift

in the VanDyck trap is $\Delta\nu_c/\nu_c \approx 1.5 \times 10^{-11}$/proton. Scaling this as $1/a^3$, the equivalent shift in our trap is $\approx 4 \times 10^{-13}$/proton. Therefore to have a shift at the reported 4.2×10^{-8} level would require approximately 10^5 protons or antiprotons.

The particle numbers typically range between 200 and 2000 antiprotons for the mass comparison measurements. Because our trap is relatively large, number dependent systematics are not significant at the level reported in this thesis.

Space Charge

In an ideal trap consisting of a perfect quadrupole field and a uniform magnetic field, no space charge shifts are observed when detecting the center of mass motion of a single trapped species, provided the cyclotron motion is excited by a constant electric field [25]. In practice, impurity ions are sometime present and the excitation fields are not uniform so that internal degrees of freedom may be excited resulting in space charge shifts. Such shifts are larger on ions of larger mass [116] and can become important for our antiproton and proton work.

Even though we perform measurements on more than one antiproton (or proton) at a time, we can minimize the effect of contaminant ions in several ways. The size of the perturbation is dependent upon the proportion of contaminant ions to the measured species and to the density of the charge. We attempt to reduce or eliminate contaminant electrons (or ions) from the antiproton (proton) clouds using the techniques described in Chapters 7 and 9. Since we have yet to try to resolve a single ion in this trap and study the small perturbations of even a single perturbing ion, we can not be absolutely certain that all possible contaminant ions are removed for our measurements. We also perform measurements only on relatively small clouds, typically 200 to 2000.

Of the few possible remaining contaminant ions, one way to attempt to see any effect is to perform measurements while varying the density. The technique of directly observing ν_c' as a function of V_0 is such a measurement.(see Section 9.1.2). In Fig. 10.12(a) we show measurements of ν_c' versus applied trapping voltage for both antiprotons (positive applied voltage) and protons (negative applied voltage). The associated linewidths of the measured resonance at ν_c' are very small on this

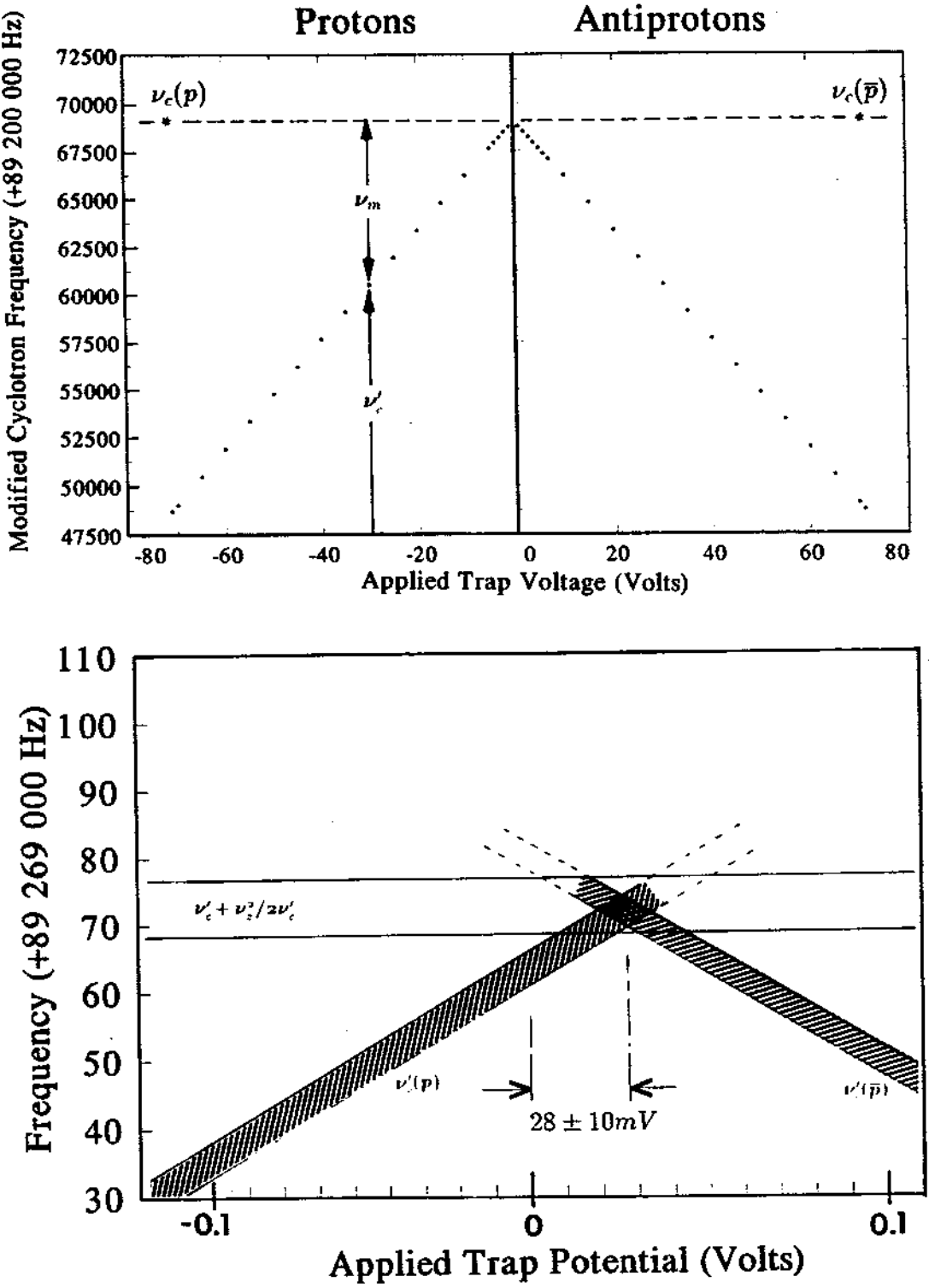

Figure 10.12: (a)Antiproton and proton cyclotron frequency ν_c' as a function of applied trapping voltage. (b) Blown up view of the extrapolated free space cyclotron frequency compared to measurments using the invariance theorem $\nu_c' + \nu_z^2/2\nu_c'$. A potential offset is evident.

scale. To first order, these points should fall on a straight line, and a linear fit gives an intercept at zero trapping potential that in principle is equal to the free space cyclotron frequency ν_c . Such an intercept can be compared with measurements of ν_c based upon making measurements of ν_c' and ν_z at a fixed voltage (about $\pm$ 71 Volts in our case) and using the invariance theorem.

Repeated measurements of ν_c' as a function of voltage and extrapolating to vanishing trapping potential showed that $\nu_c = \nu_c'$ (V_0=0) for the antiproton was slightly higher than a measurement performed at +71 Volts using $\nu_c = \nu_c' + \nu_m$. Similar measurements using protons gave a similar shift but now $\nu_c = \nu_c'$ ($V_0 = 0$) was slightly *lower* than a measurement done at -71 Volts and using $\nu_c = \nu_c' + \nu_m$. For similar space charge distributions, we would expect deviations of ν_c' to be in the *same* direction independent of the sign of the trap polarity.

Figure 10.12(b) shows the intercept region for proton and antiproton measurements taken close in time that the magnetic field has drifted only a negligible amount. The fitted lines do not intersect at the applied $V_0 = 0$ point, but rather at +28 mV. This is the same offset that was observed using the axial signals and shown in Fig. 10.7. We see that this intersection point also lies on the line $\nu_c' + \nu_m$ defined by independent measurements of the proton and antiproton at -71 Volts and +71 Volts respectively (measurements that are voltage independent).

This offset was reproducible over 3 months using 10 different clouds with different particle compositions. The experiment was warmed and recooled during this 3 months, and the magnet was de-energized and re-energized with completely new shim settings. The observed offset voltage pertains to a small change in the ideal quadrupole field. The reproducibility of the potential offset which is consistent with the offset observed axially also gives us confidence in understanding the voltage environment on the trap electrodes even with the polarity reversed.

While the intercepts of the antiproton and proton ν_c' vs. V_0 measurements provide valuable information about the true trapping potential, it is the slope which provides the most direct information on the effects of space charge (or number) dependence. This is because the space charge density can be included in expansion Eq. 9.3 with a term that goes as the trapping voltage [117]. By

examining the variation in the slopes of the proton and antiproton measurements for the ten measurements done, we put a limit on the possible effects of space charge and contaminant ions at 2×10^{-8}. These results are strong indications that possible space charge shifts are negligible in measurements with our typical cloud sizes and compositions.

While the ν_c' verse voltage technique has been presented elsewhere as an attempt to understand systematics [50], this is the first application of such a technique to the observation of a particle-antiparticle pair. It serves as a mass measurement technique, a probe for studying space charge, and a valuable tool in studying opposite polarity measurements which have been troublesome spots in high precision measurements.

Collective Modes

When ions of slightly different mass and the same charge are stored in an ion trap, a collective oscillation may be observed rather that the independent motions necessary to perform high precision mass spectroscopy. Observations have been made in a radio frequency electric quadrupole trap that suggest that precision measurements of the particle frequencies for species with nearly identical charge to mass ratios can be severly perturbed [60].

For the comparisons described in our Penning trap, only particles of similar charge can be simultaneously confined. For a positively biased trap (ring), only electrons and antiprotons are easily confined which have very different masses. For a negatively biased trap, other ions can be confined with the protons, but since only protons have a charge to mass ratio near 1 (mass in amu), collective oscillations are not a concern for small clouds of the particle species we have chosen to compare.

10.3 Particle Energy and Detection

10.3.1 Spatial Extent of Particle Motion

Due to limitations of our detection sensitivity and the fact that the detector is at a nonzero temperature, the particles have finite orbit sizes ρ_c, z, and ρ_m. The size of the excursion from the center of the trap determines the degree to which the particles sample magnetic field gradients and/or higher order non-quadrupole components in the electric field. The energy of the particles necessary to provide sufficient signal is a critical value and if too high, shifts due to special relativity may occur.

Each of the three major perturbations (electrostatic, magnetic bottle, and relativistic) produce shifts in the eigenfrequencies and each shift is linear to the classical excitation energies E_c, E_z, and E_m. The particle amplitudes are related to the particle energy in each eigenmode by

$$E_c = 1755\ \rho_c^2\ \frac{eV}{mm^2} \tag{10.15}$$

$$E_z = 0.84\ z^2\ \frac{eV}{mm^2} \tag{10.16}$$

$$E_m = -9 \times 10^{-5} \rho_m^2\ \frac{eV}{mm^2}. \tag{10.17}$$

In equilibrium, the cyclotron and axial motions are coupled to their respective resonant detection circuits which are kept near 4 K. The particle motions must be driven to higher energies during the measurements in order that these motions can be detected.

Changes in the particle energy produce corresponding shifts in the measurable eigenfrequencies $\omega \rightarrow \omega + \Delta\omega$. The leading shifts have been summarized for a single particle by Brown and Gabrielse [13]. We now consider shifts to the unperturbed eigenfrequencies which are most visible under extreme heating conditions. We emphasize that the drive levels used for the mass comparison are much less than those used to obtain the lineshapes we show here. These observations are instructive towards understanding and probing the environment in the trap.

In Fig. 10.13(a) we show three observations of the directly detected antiproton cyclotron motion after being severely heated with a strong excitation drive at ν_c'.

The line broadens as it is heated but is very asymmetric shifting towards lower frequencies (i.e $\Delta\nu_c'$ is negative for increased energy). For these cyclotron observations we infer that the heat dependent shift shown in figure 10.13 is primarily due to energy in the cyclotron motion E_c. This seems likely since the motion is excited with excitation drives at either ν_c' or $\nu_c' + \nu_m$. The cyclotron energy damps with time constant of 2.8×10^3 seconds as shown in Fig. 10.13(b). Resistive cooling by the cyclotron resonant circuit appears to be the predominant cooling mechanism. If the observed broadening is due to C_4 and B_2 as a result of a large magnetron radius we should not observe the linewidth narrow unless magnetron sideband drives are explicitly used. It is possible that the broadening results from an expansion of the cloud volume due to increased temperature, though even under heated circumstances we cannot observe any effect on the lineshape by changing B_2 with the magnet shim. Changing C_4 a large amount has some effect on the lineshape under certain conditions that seem correlated with large particle number and/or high axial energies. The general large asymmetric feature resulting from the heating normally seems unaffected by changes in C_4 within our tuning range. The assumption that the broadening (shifting) is due predominantly to energy in the cyclotron motion is also strengthened by the observation that under typical conditions (<2000 antiprotons and trap well tuned) no simultaneous heating of the axial motion is observed along with the excessive cyclotron heating (Sec. 12.3, Figs. 10.17 and 10.18).

Shifts or line broadening mechanisms are often difficult to deconvolve. To quantify the source of one perturbation requires that the others are made much less significant. Energy dependent frequency shifts of the center of mass cyclotron frequency based on single particle calculations are given by [13]

$$\left(\frac{\Delta\nu_c'}{\nu_c'}\right)_{anharm.} = \frac{6C_4}{eV_0}\left[\frac{1}{4}\left(\frac{\nu_z}{\nu_c'}\right)^4 E_c - \frac{1}{2}\left(\frac{\nu_z}{\nu_c'}\right)^2 E_z - \left(\frac{\nu_z}{\nu_c'}\right)^2 E_m\right] \quad (10.18)$$

$$\left(\frac{\Delta\nu_c'}{\nu_c'}\right)_{bottle} = \frac{1}{eV_0}\frac{B_2 d^2}{B}\left[-\left(\frac{\nu_z}{\nu_c'}\right)^2 E_c + E_z + 2E_m\right] \quad (10.19)$$

$$\left(\frac{\Delta\nu_c'}{\nu_c'}\right)_{rel.} = -\frac{1}{mc^2}\left[E_c + \frac{1}{2}E_z - \left(\frac{\nu_z}{\nu_c'}\right)^2 E_m\right] \quad (10.20)$$

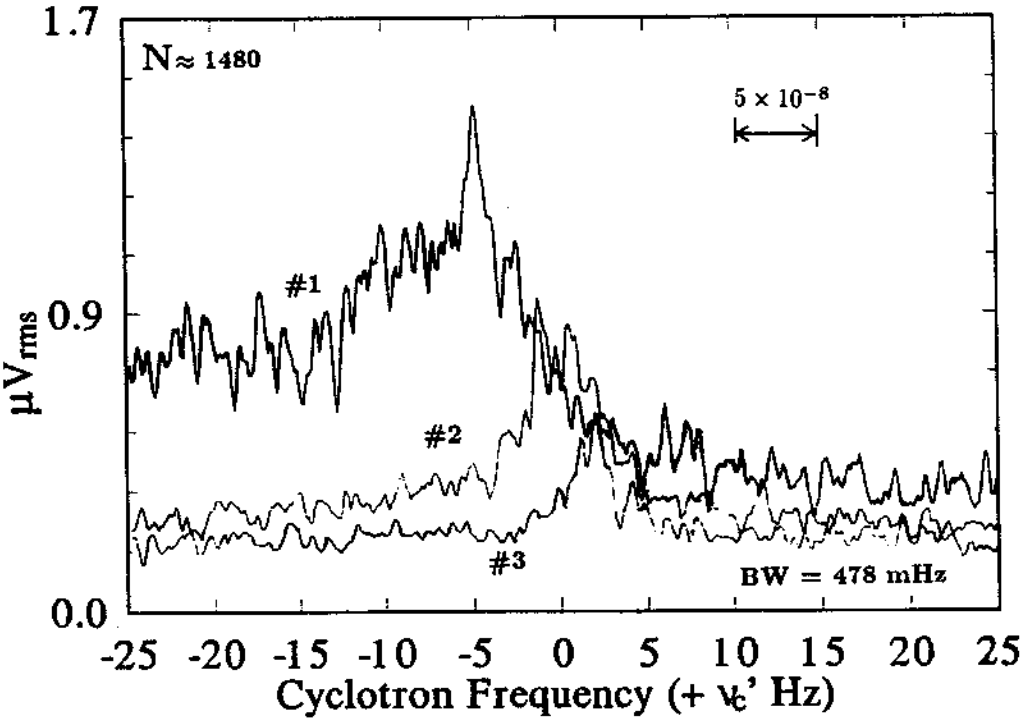

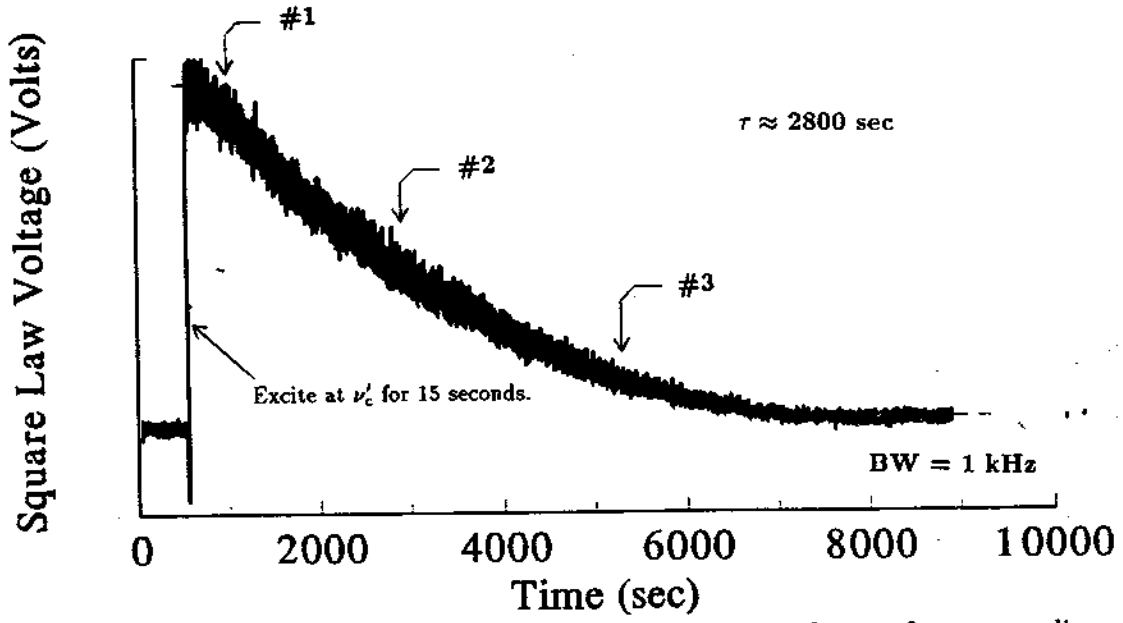

Figure 10.13: (a) Three measurements of the antiproton cyclotron frequency directly observed from a segment of the ring electrode. (b) Damping of the cyclotron center of mass motion as observed with a square law detector centered at $\nu_c(\overline{p})$.

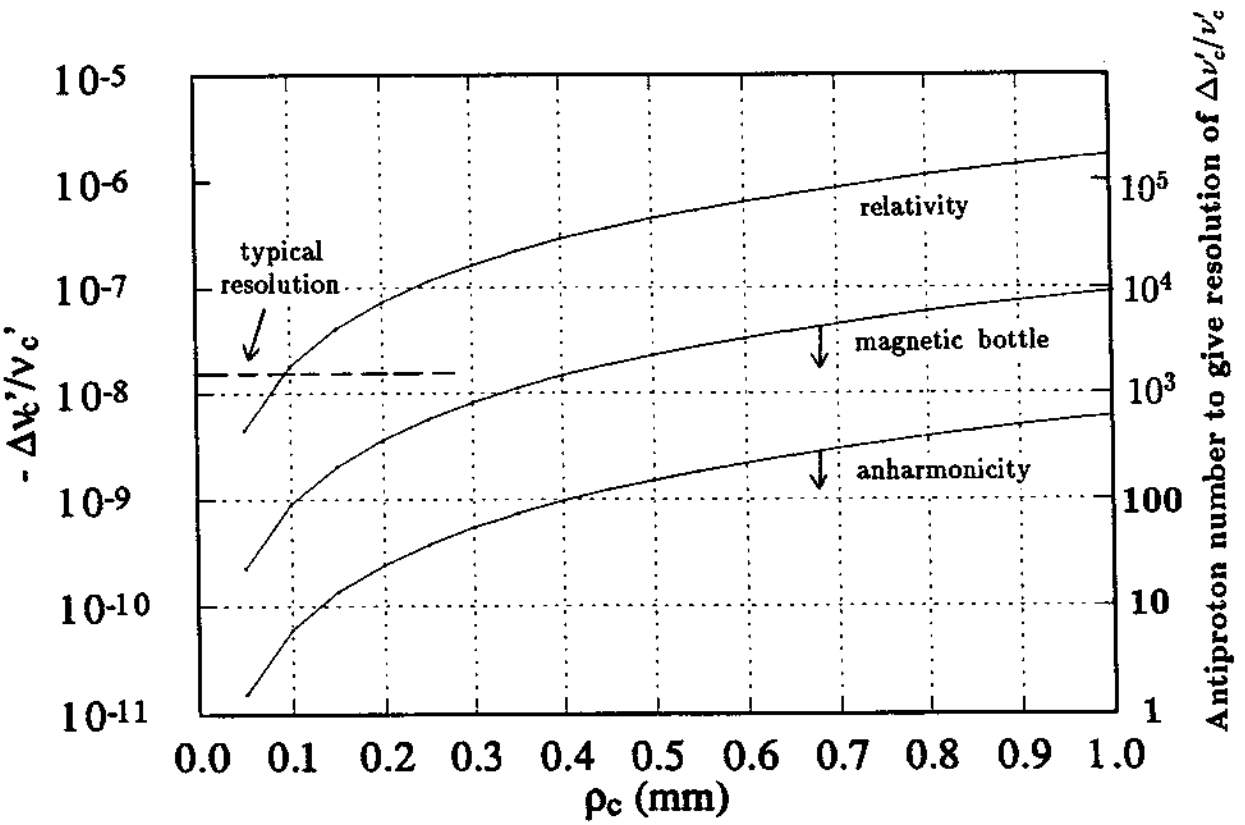

Figure 10.14: The cyclotron frequency shift $\Delta\nu_c'$ of a single antiproton as a function of the cyclotron radius due to special relativity, a magnetic bottle (+1 G/cm^2), or trap anharmonicity ($C_4 \leq -7.8 \times 10^{-4}$). The shift due to C_4 can be in either direction depending upon the compensation of the trapping potentials.

Based on the earlier arguments, let us assume that the shifts (broadening) in Fig. 10.13 are only due to energy in E_c. Then Eqs. 10.19, 10.20, and 10.20 become

$$\left(\frac{\Delta\nu_c'}{\nu_c'}\right)_{anharm.} \leq \pm 6\times 10^{-9}\rho_c^2 \ /mm^2 \tag{10.21}$$

$$\left(\frac{\Delta\nu_c'}{\nu_c'}\right)_{bottle} \leq -7.7\times 10^{-8}\rho_c^2 \ /mm^2 \tag{10.22}$$

$$\left(\frac{\Delta\nu_c'}{\nu_c'}\right)_{rel.} = -1.8\times 10^{-6}\rho_c^2 \ /mm^2, \tag{10.23}$$

$$\tag{10.24}$$

where we have used $C_4 \leq 7.8\times 10^{-4}$ and $B_2 \leq 0.84\ G/cm^2$ in the more general expressions.

In Fig. 10.14 we plot Eqs. 10.22, 10.23, and 10.24 as a function of the cyclotron radius. The most evident feature is that for our trap the bottle and anharmonic components are small enough such that the dominant shift in the cyclotron frequency resulting from energy in the cyclotron motion would be due to relativity. On the right scale of the figure we show the number of antiprotons that would contribute to a similar broadening of the linewidth. For most of our highest resolution measurements (See for example, Fig. 9.1)), the linewidth appears limited by the particle number in the trap.

To estimate the maximum possible energy in the cyclotron motion, let us assume that the observed linewidth corresponds to a relativistic shift of an ensemble of antiprotons. A resolution of 10^{-8} then corresponds to an energy of E_c on the order of 10 eV. If the observed asymmetric broadening of up to $\Delta\nu_c' \approx -400Hz$ is due to relativistic shifts, we would be dealing with a cyclotron motion center of mass energy greater than 1 keV. This seems extremely high, but may be possible since the antiprotons are only weakly damped, and under the right conditions the axial motion is essentially uncoupled from this motion. A counter arguement is that we do not observe loss of particles due to possible collisional transfer of energy into the axial motion which is bound in a well of only around 50 eV.

Heat dependent shifts are also observed in the axial motion as a function of particle temperature. In Fig. 10.15 we show an example of the axial frequency shift as a function of axial energy. The linewidth or shape does not noticeably

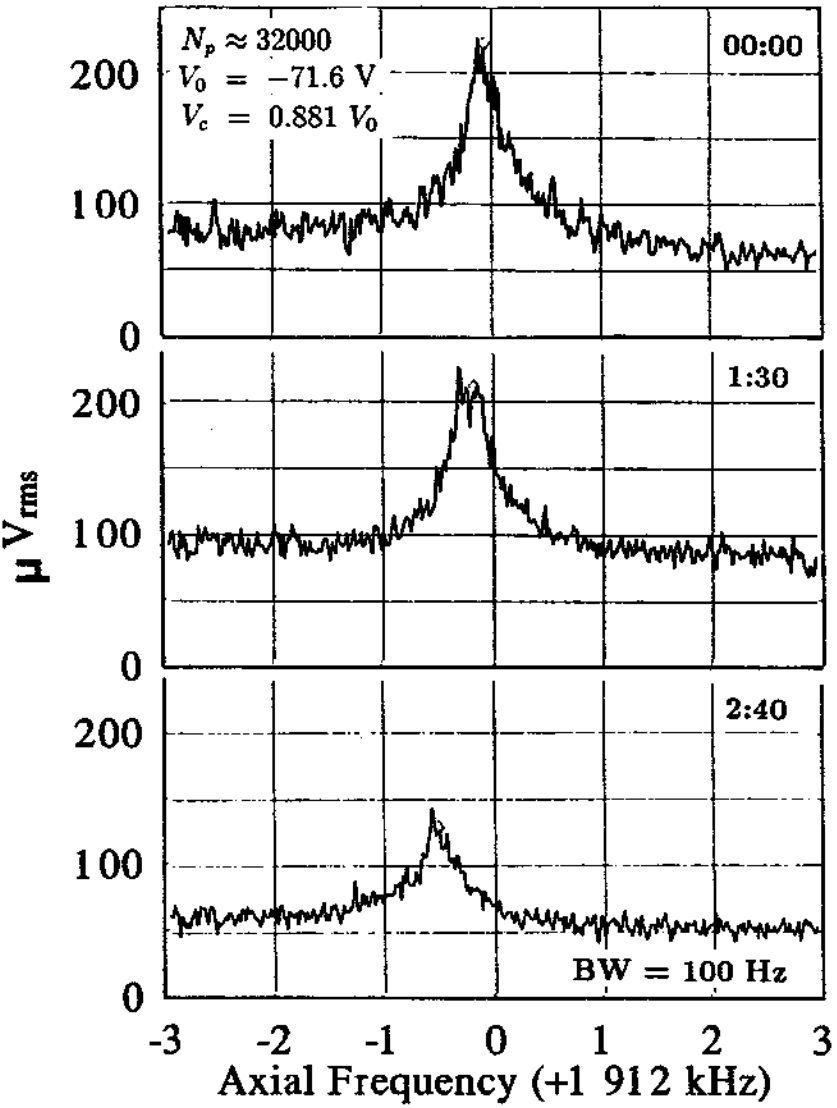

Figure 10.15: Axial shift for a fixed number of protons as a function of temperature in the axial motion

change as it damps indicating the linewidth is limited by particle number in this case. Shifts in the axial frequency for a single particle can also be expressed in terms of the center of mass energy in the three motions. Shifts due to the major perturbations are [13].

$$\left(\frac{\Delta\nu_z}{\nu_z}\right)_{Anharm.} = \frac{6C_4}{eV_0}\left[-\frac{1}{2}\left(\frac{\nu_z}{\nu_c'}\right)^2 E_c + \frac{1}{4}E_z + E_m\right] \tag{10.25}$$

$$\left(\frac{\Delta\nu_z}{\nu_z}\right)_{bottle} = \frac{1}{eV_0}\frac{B_2 d^2}{B}[E_c - E_m] \tag{10.26}$$

$$\left(\frac{\Delta\nu_z}{\nu_z}\right)_{rel.} = -\frac{1}{mc^2}\left[\frac{1}{2}E_c + \frac{3}{8}E_z - \frac{1}{4}\left(\frac{\nu_z}{\nu_c'}\right)^2 E_m\right]. \tag{10.27}$$

The shifts in Fig. 10.15 correspond to $\Delta\nu_z/\nu_z \approx 3\times10^{-4}$ which is much too large to be due to relativity. The shift is most likely due to anharmonicity. As seen in Eq. 10.25 the axial shift is more sensitive to the axial energy than the cyclotron energy by a factor of $2(\nu_z/\nu_c')^2 \approx 1/1250$. In general, the two largest observed shifts in the axial signal are due to this heat dependent shift (up for increased energy) or to a change in particle number (down for increased number).

In Chapter 6 (for example, see Fig. 6.4), the need to incorporate anharmonicity in order to increase detection sensitivity of the excited electron cyclotron motion was demonstrated. When the trap was tuned so that $C_4 \approx 0$, and the magnetic bottle was minimized, the observed shifts in $\Delta\nu_z$ for increased E_c were very small. By increasing the leading anharmonic component to $C_4 \approx 5.6\times10^{-3}$, cyclotron resonances could easily be observed as a shift in the axial frequency.

With the antiprotons and protons we can observe the cyclotron frequency directly. Figures 10.13 and 10.15 show how the signal amplitudes and linewidths vary as function of heat in the cyclotron and axial motions. In Fig. 10.16, 10.17, and 10.18 we show three separate situations where the cyclotron signal and axial signal are simultaneously recorded. In the first case, both degrees of freedom show some heating. After the signals damp, the number of antiprotons is then reduced and the cyclotron motion is reheated with an excitation drive near ν_c'. Fig. 10.17 shows that the cyclotron motion is severly heated, but that the axial signal is much less so. Figure 10.18 shows the same cloud about one-half hour

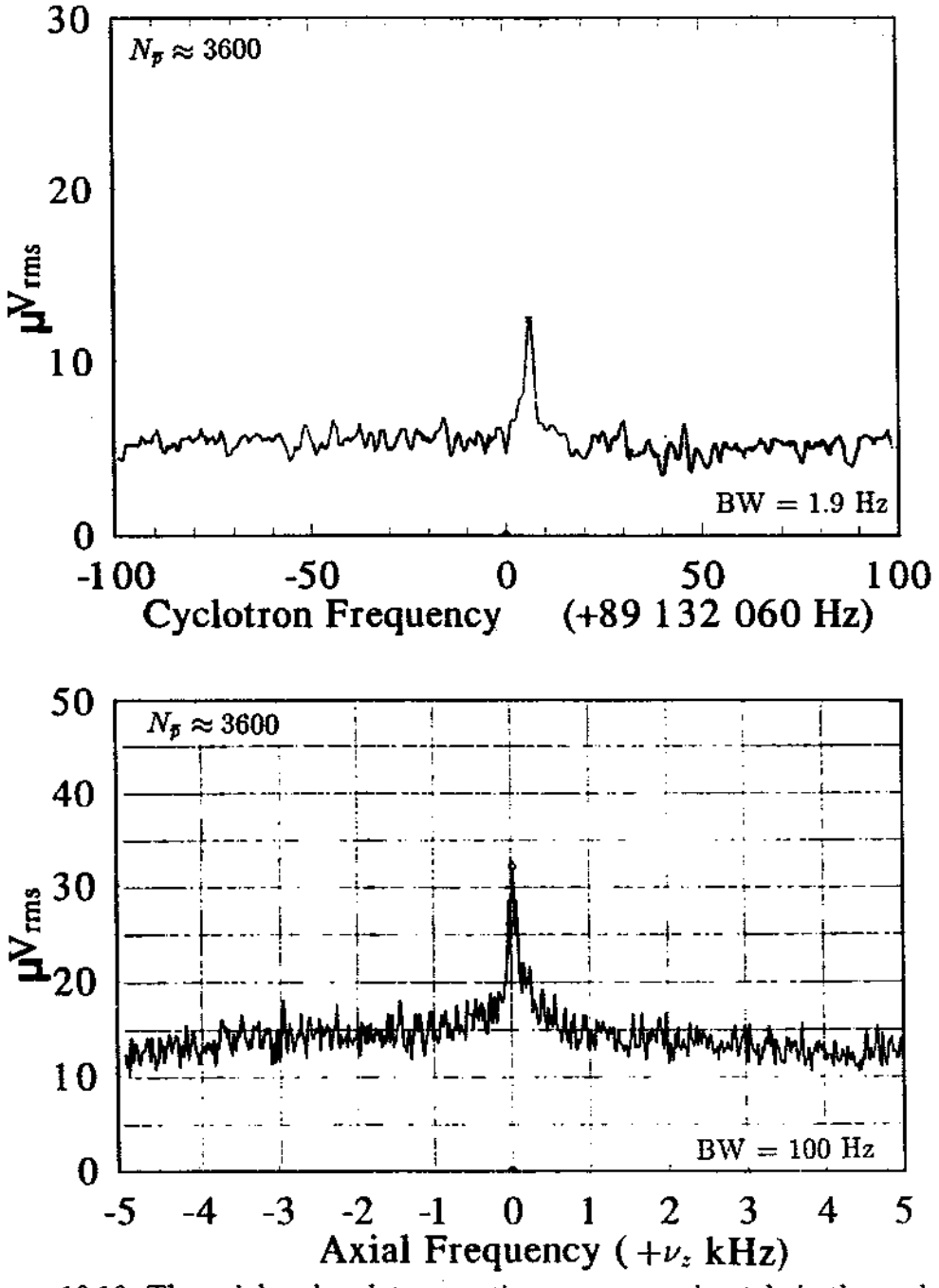

Figure 10.16: The axial and cyclotron motions are approximately in thermal equilibrium.

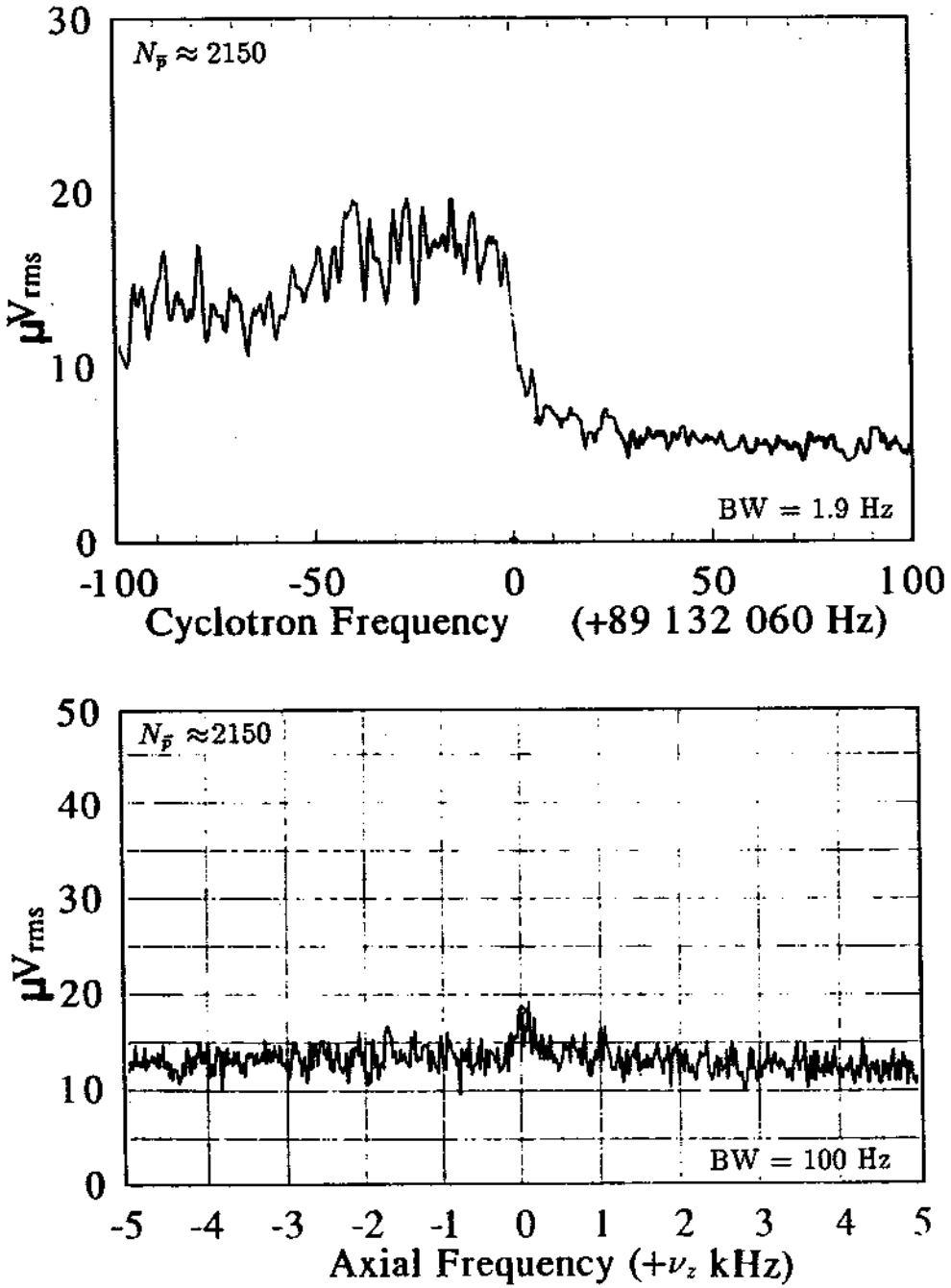

Figure 10.17: Large amount of heat in the cyclotron motion while the axial motion remains cool.

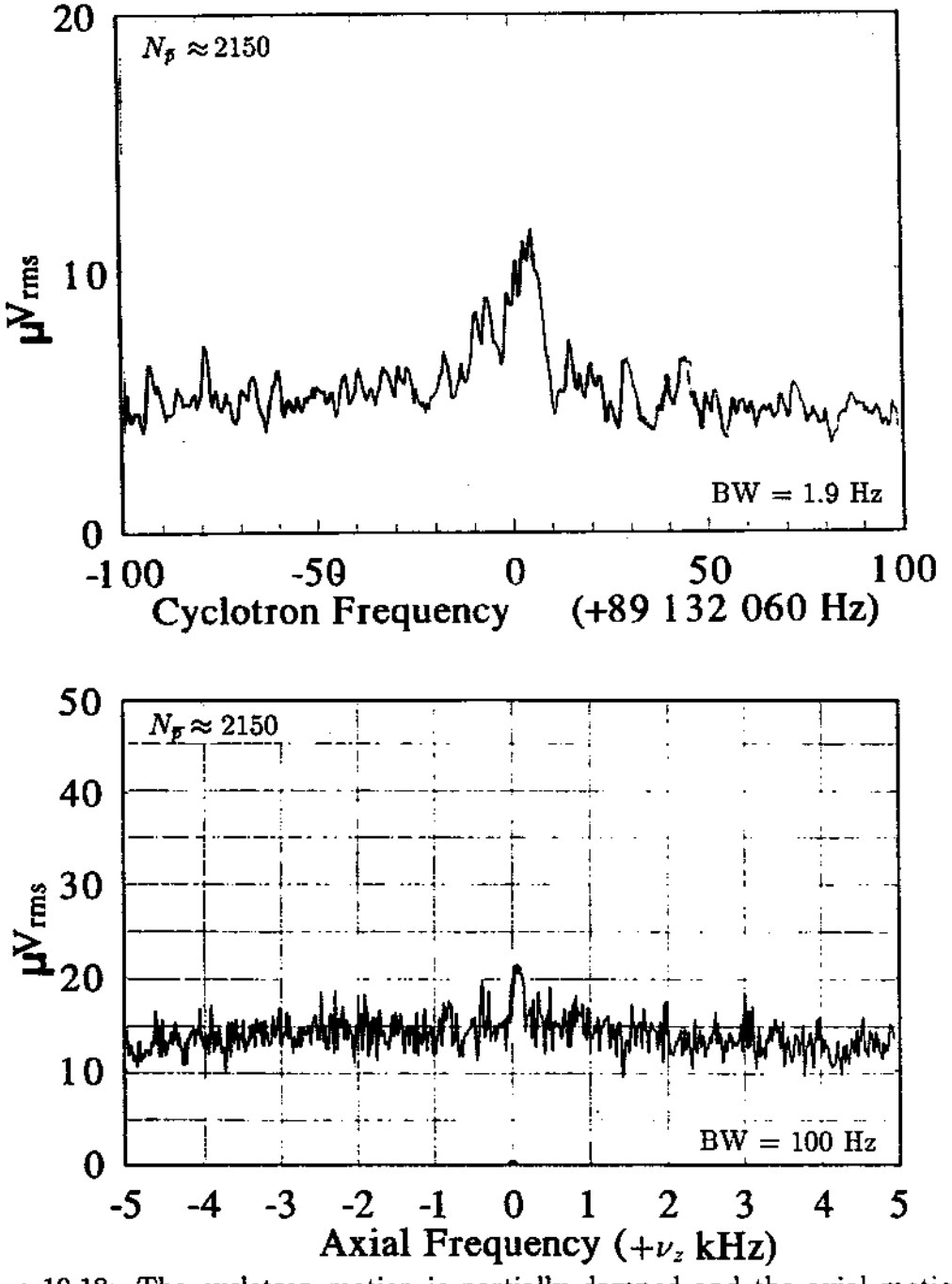

Figure 10.18: The cyclotron motion is partially damped and the axial motion remains cold.

later as the cyclotron motion has apparently resistively damped. The axial signal shows little change. The trap was optimally tuned for these three situations. By mistuning the trap, energy from the hot cyclotron motion can be coupled to the axial motion, though in general if the particle number is low and C_4 minimized, large heating of the cyclotron motion is observable without a corresponding rise in the axial energy as seen in Figs. 10.17 and 10.18. For higher numbers, the axial and cyclotron motions are much more coupled presumably via collisions.

10.3.2 Detection Effects

Shifts From Oscillator Coupling

Coupling between the particle oscillator and the detection resonant circuit can cause a shift in the particle eigenfrequency. The pulling of the particle frequency can be significant at high precisions. For direct detection of the cyclotron motion the pulling of the coupled circuits directly contributes to the uncertainty. For our detection parameters and detuning, the pulling on ν_c' for our typical number of antiprotons is estimated to be about 1 Hz. For similar mass particles, a comparison of the cyclotron frequencies will be relatively insensitive to such pulling since it nearly cancels when we take the ratio. For the proton to electron comparisons the pulling uncertainty can become significant depending on the mistuning. For the measurements reported in this thesis, ν_c' is substantially detuned from the center frequency of the detection resonant circuit and the pulling is $\leq 10^{-8}$.

Frequency Standard

All of the frequency synthesizers are frequency locked using the 10 MHz output of a Ball Efratom Modular Rubidium Frequency Standard (Model MRT-LN). Specifications at 5 MHz report a long term time drift of

$$\Delta\nu/\nu \leq 1 \times 10^{-11}/month, \tag{10.28}$$

The effects of frequency variation due to temperature and magnetic field fluctuations are $\leq 10^{-10}$ (from -10° C to +50° C) and $\leq 3 \times 10^{-11}$/G respectively.

10.4 Systematic Summary

In Table 10.2 we summarize and place limits on possible systematic effects described in this chapter. Because of the large trap, the small bottle, and the ability to tune away anharmonicity, most of the systematic limits summarized are insignificant at the 10^{-8} level. To account for the limits summarized here we add the fractional uncertainty

$$\sigma_{sys} = 2 \times 10^{-8} \tag{10.29}$$

to our results presented in Chapter 11.

The cyclotron and axial lineshapes for the antiproton(proton) and the cyclotron lineshape for the electron are not totally understood as demonstrated by the hight heat shifts. Since the resolution is so good for low heat situations, we choose not to split the measured resonance line for any of the observations used for the mass comparison. Thus we assign the fractional uncertainty of

$$\sigma_{width} = 2.8 \times 10^{-8}. \tag{10.30}$$

associated with the typical linewidth of 2.5 Hz during our frequency measurements.

Table 10.2: Summary of Systematic Errors ($\Delta\nu_c/\nu_c$)

MAGNETIC FIELD DEVIATIONS	
Homogeneity	
Linear Gradient ($< 1.6 \times 10^{-8}$/mm)	$\leq 3 \times 10^{-10}$ (E=0.3 meV)
Bottle ($< 1.7 \times 10^{-7}$/mm^2)	$\leq 5 \times 10^{-11}$ (E=0.3 meV)
Drift	
Long Term	$< 8 \times 10^{-10}/hr$
Field Fluctuations	
Bending Magnets	$< 1 \times 10^{-8}$
PS/LEAR	6×10^{-9}
QUADRUPOLE FIELD DEVIATIONS	
Trap Geometry	
Distortions, Misalignment ($\epsilon \leq 1\%, \theta \leq 1^\circ$)	$\leq 4 \times 10^{-11}$
Effects From Electrode Potentials	
Stability of Trap Potential ($\Delta V_0 << 150\mu$V)	$< 2 \times 10^{-8}$
Tuning and Harmonicity ($C_4 \leq 7.6 \times 10^{-4}$)	$< 9 \times 10^{-11}$ (E=0.3 meV)
Effects From the Presence of Other Particles	
Number Dependence ($\Delta\nu_c/\nu_c \approx 5 \times 10^{-13}/\overline{p}$)	$< 10^{-9}$ (for 3000 $\overline{p}$)
Space Charge (slope average of ν_c' *vs.* V_0)	$< 2.0 \times 10^{-8}$
DETECTION RELATED EFFECTS	
Amplifier Pulling	$< 10^{-8}$
Frequency Standard Stability	$< 10^{-11}$
Relativistic Shift	2×10^{-13} (E=0.3 meV)